

# Design and expected performance of a novel hybrid detector for very-high-energy gamma-ray astrophysics

P. Assis<sup>a,b</sup>, U. Barres de Almeida<sup>c</sup>, A. Blanco<sup>d</sup>, R. Conceição<sup>a,b</sup>, B. D’Ettorre Piazzoli<sup>e</sup>, A. De Angelis<sup>f,g,b,a</sup>, M. Doro<sup>h,f</sup>, P. Fonte<sup>d</sup>,  
L. Lopes<sup>d</sup>, G. Matthiae<sup>i</sup>, M. Pimenta<sup>b,a</sup>, R. Shellard<sup>c</sup>, B. Tomé<sup>a,b</sup>

<sup>a</sup>LIP Lisboa, Portugal

<sup>b</sup>IST Lisboa, Portugal

<sup>c</sup>CBPF, Rio de Janeiro, Brazil

<sup>d</sup>LIP Coimbra and University of Coimbra, Portugal

<sup>e</sup>Università di Napoli “Federico II” and INFN Roma Tor Vergata, Italy

<sup>f</sup>INFN Padova, Italy

<sup>g</sup>Università di Udine, Italy

<sup>h</sup>Università di Padova, Italy

<sup>i</sup>INFN and Università di Roma Tor Vergata, Roma, Italy

---

## Abstract

Current detectors for Very-High-Energy  $\gamma$ -ray astrophysics are either pointing instruments with a small field of view (Cherenkov telescopes), or large field-of-view instruments with relatively large energy thresholds (extensive air shower detectors).

In this article, we propose a new hybrid extensive air shower detector sensitive in an energy region starting from about 100 GeV. The detector combines a small water-Cherenkov detector, able to provide a calorimetric measurement of shower particles at ground, with resistive plate chambers which contribute significantly to the accurate shower geometry reconstruction.

A full simulation of this detector concept shows that it is able to reach better sensitivity than any previous gamma-ray wide field-of-view experiment in the sub-TeV energy region. It is expected to detect with a  $5\sigma$  significance a source fainter than the Crab Nebula in one year at 100 GeV and, above 1 TeV a source as faint as 10% of it.

As such, this instrument is suited to detect transient phenomena making it a very powerful tool to trigger observations of variable sources and to detect transients coupled to gravitational waves and gamma-ray bursts.

*Keywords:* Gamma-ray astronomy, Extensive air shower detectors, Transient sources, Gamma-ray bursts

---

## 1. Introduction

High energy gamma rays are important probes of extreme, non thermal, events taking place in the universe. Being neutral, they can cover large distances without being deflected by galactic and extragalactic magnetic fields. This feature enables the direct study of their emission sources. The gamma emission is also connected to the acceleration of charged cosmic rays and to the production of cosmic neutrinos. Gamma-rays can also signal the existence of new physics at the fundamental scales, namely by the annihilation or decay of new types of particles, as it is the case for dark matter particles in many models. This motivation, associated to the advances of technology, has promoted a vigorous program of study of high energy gamma rays, with important scientific results (see [1, 2, 3, 4] for a summary of the main achievements).

The detected sources of cosmic gamma-rays above 30 MeV are concentrated around the disk of the Milky Way; in addition there is a set of extragalactic emitters. About 3000 sources

emitting above 30 MeV were discovered, mostly by the Large Area Telescope (LAT) detector [5] onboard the *Fermi* satellite, and some 200 of them emit as well above 30 GeV [6] (see Fig. 1) - the region which is labeled the Very High Energy (VHE) region.

Our Galaxy hosts about half of the VHE gamma-ray emitters [7] and most of them are associated to supernova remnants of various classes (shell supernova remnants, pulsar-wind nebulae, etc.). The remaining emitters are extragalactic. The angular resolution of current detectors, which is slightly better than  $0.1^\circ$ , does not allow to assign the identified extragalactic emitters to any particular region in the host galaxies; however, there is some consensus that the signals detected from the Earth must originate in the proximity of supermassive black holes at the center of the galaxies [8].

Still, many problems remain open, of which we may mention:

- *The origin of cosmic rays* – supernova remnants (SNRs) are thought to be the sites for the acceleration of protons up to few PeV. However, the mechanism of acceleration of particles to energies of that order is still to be established experimentally. The study of the photon yield from Galactic sources for energies larger than 100 GeV and all the

---

\*Corresponding authors

Email addresses: ruben@lip.pt (R. Conceição),  
alessandro.deangelis@pd.infn.it (A. De Angelis),  
shellard@cbpf.br (R. Shellard)

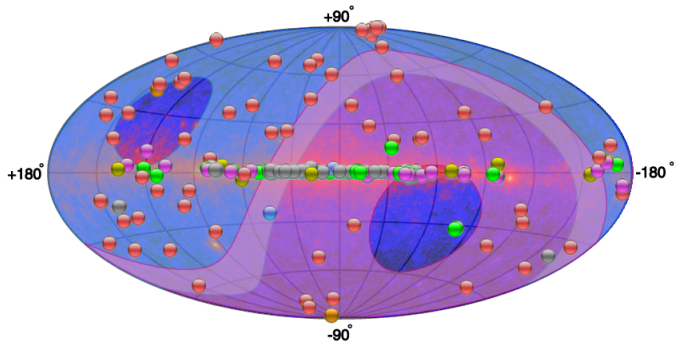


Figure 1: Sources of VHE emission displayed in galactic coordinates. The background represents the high-energy gamma-rays detected by *Fermi*-LAT. The clear blue (dominant on the left side) area corresponds to the visible region within  $30^\circ$  of the zenith from a detector at a latitude of 22 degrees in the Northern hemisphere while the pink (dominant on the right side) shows the corresponding region in the Southern hemisphere. From <http://tevcat.uchicago.edu/>, June 2016.

way up to PeV, might solve the problem (see for example [9]). Actually, photons, which come from  $\pi^0$  decay, correspond to hadronic cascades initiated at energies at least an order of magnitude larger.

- *The propagation of gamma-rays* – tells us about their interaction with the cosmic background radiation and is a probe to cosmology themes.
- *New physics* – the ultimate nature of matter and of physics beyond the Standard Model, dark matter or new particles in general, the energy density of the vacuum or even quantum gravity may leave imprints in the spectrum of VHE gamma rays. High-energy gamma-ray astrophysics is sensitive to energy scales important for particle physics. For instance, cold dark matter is expected to be found in the 100 GeV scale; supersymmetric particles could appear at the TeV scale; and the Planck scale (an energy  $\sim 10^{19}$  GeV, corresponding to a mass  $\sqrt{\hbar c/G}$ ) could be probed indirectly (for discussion see for example [1]).
- *Transients* – Many VHE sources are characterised by variability, and it is important to be able to detect and measure the corresponding flares. Such flares have a duration that can go from few seconds – like for the short gamma-ray bursts or the expected counterparts of gravitational waves – to minutes for the long gamma-ray bursts, to minutes, hours or even days for the accretion flares of blazars (see e.g. [10] and references therein).

The layout of this paper is the following. In the Introduction we have briefly presented the field of very-high-energy gamma-ray astrophysics. In Section 2 we outline the characteristics of the existing detectors, and we explain why a large field-of view detector is needed. In Section 3 we make a case study with a possible design for such a detector. In Section 4 we describe the characteristics of the gamma-ray signal and of its background, and the various Monte Carlo samples used in the analysis of the

performance of the proposed detector. In Section 5 we evaluate the performance of such a new detector using the simulation. We conclude the paper with final remarks and a summary in Section 6.

## 2. Detection of gamma rays

The direct detection of primary X/ $\gamma$ -rays is only possible using satellite-based detectors since the radiation is absorbed in the atmosphere. However, the cost of space technology limits the size of satellite-borne detectors to, roughly, areas of about one square meter. The largest and most sensitive space-based gamma detector is *Fermi*, with its high-energy sub-detector, the LAT, with an area of about  $3 \text{ m}^2$ , and an effective area – the product of the geometrical area by the energy dependent detection efficiency – of about  $1 \text{ m}^2$  for a gamma-ray with an energy of 1 GeV [11].

If the energy of a primary cosmic photon is above some tens of GeV part of the products of the air shower, initiated by the interaction of the photon with the atmosphere, can reach the Earth surface. Ground-based detectors have a large effective area, so their sensitivity is high, however they are subjected to a large amount of background events, typically charged cosmic rays. They outperform satellite-based detectors, like the *Fermi*-LAT, in the VHE energy region. The placement of such detectors at high altitude reduces the amount of atmospheric absorption, allowing to reach lower primary energies.

VHE gamma ground based detectors can be divided in two major classes: the Extensive Air Shower (EAS) arrays and the Cherenkov telescopes.

### 2.1. EAS arrays

A typical EAS array consists of a large number of detectors that record the secondary shower particles that reach the ground. Although the energy resolution is poor, it has a very high duty cycle and a large field of view. Currently, the energy threshold of EAS detectors is at best in the 0.5 TeV - 1 TeV range. At such energies, fluxes are low and large surfaces of the order of  $10^4 \text{ m}^2$  are required. This can be achieved:

- either by using a sparse array of scintillator-based detectors, as for example in the Tibet-AS [12] (for an energy of 100 TeV there are about 50 000 electrons in the shower at mountain-top altitudes), which has already finished operations;
- or by a dense coverage of the ground, to ensure efficient collection and hence lower the energy threshold. The ARGO-YBJ detector [13], an array of resistive plate chambers (RPC) at the Tibet site, followed this approach.

The largest EAS detector, dedicated to (very) high-energy gamma-rays, presently in operation is the High Altitude Water Cherenkov (HAWC) array [14, 15] which is in Mexico at an altitude of 4100 m.

The main problem in this class of detectors is the background rejection, since the flux of charged cosmic rays above 0.5 TeV

is about a thousand times larger than that from the most intense gamma source. Muon detectors are useful instruments to reduce background. Background rejection can be otherwise based on the reconstructed shower topology, which is different for gamma-initiated atmospheric showers and for hadron-initiated showers. The direction of the primary particles is estimated from the arrival times with an angular precision which can reach about 1 degree at best.

There are new plans to build or expand new, larger and more sensitivity, experiments, for instance, the LHAASO detector [16], with an area of  $\sim 90\,000\text{m}^2$ , which is planned to be built in China. Another EAS gamma-ray experiment extension, worth to be mentioned due to its hybrid detector nature, is the TAIGA experiment [17]. One interesting aspect is that all the VHE gamma-ray EAS arrays are located at the North hemisphere.

## 2.2. Cherenkov telescopes

The Imaging Atmospheric Cherenkov Telescopes (IACTs) detect the Cherenkov light produced by the atmospheric shower during its development.

The IACTs have currently reached their third generation. They have a low duty cycle (about 1000 to 1500 hours per year) as they can only operate in moonless nights or with moderate moon light and without clouds. These detectors have typically a small field-of-view (FoV) below  $5^\circ \times 5^\circ$ . On the other hand, these kind of detectors present a high sensitivity and an energy threshold as low as 30 GeV for the present generation. In fact, most of the experimental results on VHE photons came from IACT observations.

Similarly to EAS arrays, also these experiments have to deal with huge hadronic backgrounds. This is achieved through the exploration of the shower shape as recorded in the camera [18].

In order to improve the background rejection, and obtain a better angular and energy resolution, the most recent IACT experiments use systems of more than one Cherenkov telescope.

Currently, there are three large operating IACTs: the High Energy Stereoscopic System (H.E.S.S.), the Major Atmospheric Gamma-ray Imaging Cherenkov Telescope (MAGIC), and the Very Energetic Radiation Imaging Telescope Array System (VERITAS), the first one is located in the southern hemisphere, and the two latter in the northern hemisphere.

The typical sensitivities of these IACTs are such that a source with a luminosity of 1% of Crab can be detected at a  $5\sigma$  significance in 50 hours of observation for energies above 50-100 GeV.

The Cherenkov Telescope Array, CTA, is an array of IACTs that will improve the sensitivity to point sources by nearly one order of magnitude to its predecessors. Having a very broad science case, it will be able to survey the whole sky through dedicated scans [19]. This experiment will also be able to extend the current IACT sensitivity up to 100 TeV and have a broader field-of-view (up to 10 degrees). However, it has a lower duty cycle when compared to EAS-arrays and a still narrower field of view which limits the detection of transient phenomena and the following of extended sources for long term observations.

Table 1 compares the main characteristics of currently operating satellite-borne and ground based detectors.

## 3. Design of a novel detector

Either technique for ground-based observation of gamma-ray sources has clearly advantages and drawbacks. In this paper we propose a novel hybrid detector designed as a “dense” array for a surface of  $20\,000\text{m}^2$ , that can solve some of the limitations of the present gamma-ray experiments. The requirements of a detector, able to detect possible transients with a large enough sensitivity, would imply a high duty cycle and a large field of view. Moreover, the detector should be able to cover the energy range between 100 GeV and a few TeV.

The detector we are going to propose can be the kernel for an EAS detector in which it is complemented by an external sparse detector array covering some  $100\,000\text{m}^2$  to increase the sensitivity above 5 TeV and to make it comparable with the foreseen extension of HAWC and with the planned LHAASO detector.

ARGO and HAWC have both explored the concept of a single detector composed by: either a large carpet of RPCs with a very good time and space resolutions (ARGO), or a large set of Water Cherenkov Detectors WCD, each one with large volume of water (HAWC). The ARGO approach relies on a detailed knowledge of the charged particle pattern of the air showers at ground. The HAWC approach relies on the knowledge of the electromagnetic energy contents of the air shower integrated over a large size region at ground combined with a good discrimination power for single muons.

In this paper we argue that a hybrid concept composed by a carpet of low-cost RPCs on top of WCDs (or other Cherenkov detectors based on glass or lead glass) of reasonably small dimensions, benefits from the main advantages of both approaches and can reach a much better sensitivity at the lowest energies (around 100 GeV). This detector should be placed at high altitude (we assume 5200 m a.s.l. in this paper).

Our basic element used in this simulation, the station (Fig. 2), is constructed by putting together one WCD, with a rectangular horizontal surface of  $3\text{m} \times 1.5\text{m}$  and a depth of 0.5 m, with signals read by PMTs at both ends of the smallest vertical face of the block. The inner walls of the WCD are painted white to maximize the light collection. On top of the WCD there are two RPCs, each with a surface of  $(1.5 \times 1.5)\text{m}^2$  and with 16 charge collecting pads. Each RPC is covered with a thin (5.6 mm) layer of lead, to provide the conversion of shower photons that have a stronger correlation with the primary direction than the shower electrons.

The full detector (Fig. 3) is deployed as an array of individual stations set in long lines with each touching the other on their largest dimension. The row of lines of detectors are separated by a small distance (roughly 0.5 m) to allow access to service the PMTs and the RPCs. This arrangement allows for a compact array and for a scaling of the full detector. The performance results presented herein are based on a baseline configuration with an effective area of around  $20\,000\text{m}^2$ . The station detectors are placed in such a way that the full array is a circle with radius  $\approx 80\text{m}$ .

The proposed RPCs are of the MARTA type (see [20]) which have been developed in the last four years at LIP in Coim-

Quantity	<i>Fermi</i> -LAT	IACTs	EAS
Energy range	20 MeV–200 GeV	100 GeV–50 TeV	400 GeV–100 TeV
Energy res.	5-10%	15-20%	~ 50%
Duty Cycle	80%	15%	> 90%
FoV	$4\pi/5$	5 deg $\times$ 5 deg	$4\pi/6$
PSF	0.1 deg	0.07 deg	0.5 deg
Sensitivity	1% Crab (1 GeV)	1% Crab (0.5 TeV)	0.5 Crab (5 TeV)

Table 1: A comparison of the characteristics of *Fermi* LAT, of the present IACTs and of a typical EAS particle detector array for (very) high-energy gamma-ray detection. Sensitivity is computed over one year for *Fermi* and the EAS, and over 50 hours for the IACTs.

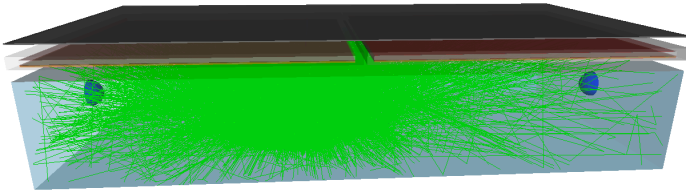


Figure 2: Basic detector station, with one WCD covered with RPCs and a thin slab of lead. The green lines show the tracks of the Cherenkov photons produced by the electron and positron from the conversion of a photon in the lead slab.

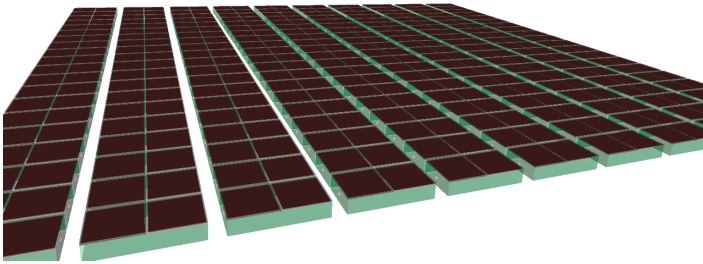


Figure 3: Detail of the layout of the detector used in the case study.

bra, Portugal, and successfully tested at Pierre Auger site in Malargüe, Argentina. These RPCs were designed to work at low gas flux, (1-4) cc/min, at harsh outdoor environment, and demanding very low maintenance services. Their intrinsic time resolution was measured to be better than 1 ns.

#### 4. Signal, background and simulation tools

We have performed a Monte Carlo simulation of the detector to evaluate its performance.

For the simulation of atmospheric showers we use the CORSIKA (COsmic Ray SIMulations for KAScade) (version 7.5600) program having the electromagnetic interaction been treated by the EGS4 routines [21]. The model to describe hadronic interactions is FLUKA [22, 23], together with the QGSJet-II.04 [24] model for high-energy interactions.

Gamma and proton primaries are simulated with a power-law energy spectrum with index -1.0. The energy of the simulated

showers ranges between 10 GeV and 300 TeV. Gamma rays are simulated as coming from a point-like source at a zenith angle of  $10^\circ$ , while protons are simulated with incoming directions spanning the range from  $5^\circ$  to  $15^\circ$  in zenith angle.

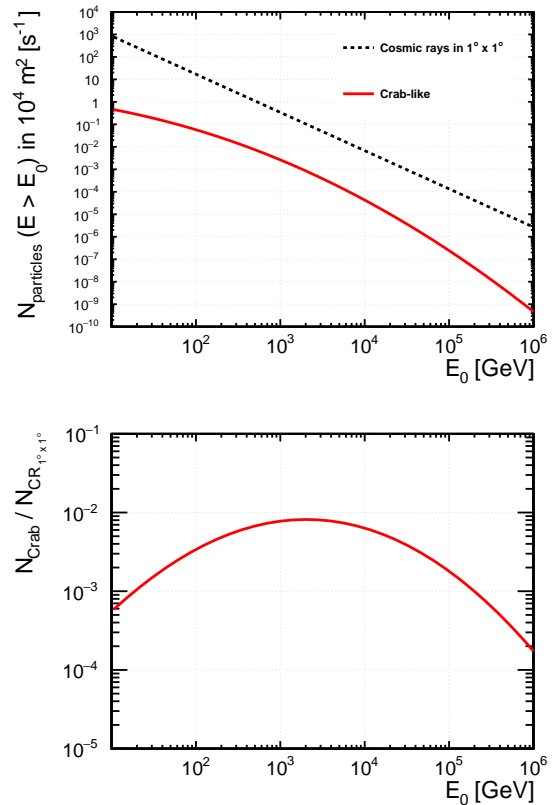


Figure 4: Top: Rate of particles above a given energy on a perpendicular surface of  $10000 \text{ m}^2$ , expected from a Crab-like source (solid line) and from the cosmic-ray proton background in one square degree (dashed line). Bottom: ratio signal/background from the above plot.

Once atmospheric showers have been simulated and the information of the electrons and photons reaching a height of 5200 m a.s.l. is recorded, we simulate the response of the detector stations using the GEANT4 [25, 26] toolkit.

Each simulated shower is reprocessed 100 times, with a new core position randomly set in each realisation. The core sampling area depends on the shower energy to account for the size

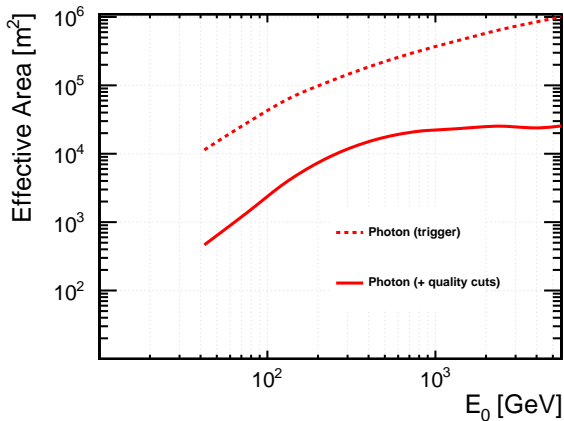


Figure 5: Effective area at trigger level (dashed curves) and after the selection used for the shower direction reconstruction (solid curves), for gamma-ray initiated showers. No g/h separation cuts were applied to any of the curves.

of it. Showers with energies around 100 GeV are uniformly sampled from the center of the array up to 600 m, while showers of 300 TeV are randomised up to 2500 m.

In the baseline simulation of the WCD units, the photomultipliers have a diameter of 15 cm. The maximum quantum efficiency is 30% at  $\lambda \sim 420$  nm. The inner walls of the tanks are covered with a white diffusive surface in order to increase the light collection. The specular and diffusive properties of this layer are accounted for, as well as its wavelength dependence. In more detail, the reflectivity was taken to be 95%, for  $\lambda > 450$  nm, of which 80% is diffusively reflected and 20% is reflected according to a Gaussian angular distribution around the specular reflection direction, with a characteristic width of  $\sigma_\alpha \sim 0.2^\circ$ . The detailed structure and materials of the RPC are also described in the simulation. In particular the information concerning the ionising energy depositions in the gas is recorded for subsequent processing.

The response of the tanks was studied for single vertical particles injected uniformly over the top surface. The mean number of photoelectrons for 20 MeV photons, the median photon energy at about 10 m from the shower core, is 15 photoelectrons, while for relativistic muons it is 230 photoelectrons.

In order to evaluate the performance of the detector, we consider a source with an emission energy distribution like the Crab Nebula. This nebula ( $\sim 2$  kpc away) is the brightest steady source detected in VHE gamma-rays [27], and as such is used as a *standard candle* in VHE gamma-ray astronomy. Occasionally the Crab flux can vary in the GeV range as recently observed [28, 29].

The *stationary* flux from the Crab Nebula follows, according to the measurements from MAGIC [30], a law

$$\frac{dN_\gamma}{dE} \simeq 3.23 \times 10^{-7} \left( \frac{E}{\text{TeV}} \right)^{-2.47-0.24\left(\frac{E}{\text{TeV}}\right)} \text{TeV}^{-1} \text{s}^{-1} \text{m}^{-2}. \quad (1)$$

The spectral energy distribution of the background cosmic-

rays can be obtained from

$$\frac{dN}{dE} \simeq I_0 \left( \frac{E}{\text{GeV}} \right)^{-2.7} \text{GeV}^{-1} \text{s}^{-1} \text{sr}^{-1} \text{m}^{-2}; \quad (2)$$

which is valid from some 10 GeV to a few hundreds of TeV [31].

The rate of photons from a Crab-like source, above a given energy threshold, is shown in Fig. 4 and compared to the background from cosmic-ray protons in a square degree.

The photon and proton showers, simulated with an energy spectrum with index -1.0, are weighted by  $E_0 \times f(E_0)$ , where  $f$  is the differential energy spectrum in Eqs. 1 and 2, respectively, and  $E_0$  is the energy of the primary particle.

## 5. Estimated performance

### 5.1. Effective area

We use a trigger selection which requires that at least three stations have detected a signal; the trigger condition for each station requires at least 5 photoelectrons in each photomultiplier. Although a detailed study of the trigger is out of the scope of this paper, it is expected that the trigger for such an experiment will be composed by a central hardware trigger followed by additional trigger levels which could be built up either by hardware or software. These trigger levels can be tuned as a function of the intended analysis. The effective area at trigger level, i.e., the integral of the surface times the trigger efficiency, is shown in Fig. 5 for gamma-ray initiated showers. This plot is shown requiring only the trigger and applying the analysis quality cuts that will be described in the following sections. In particular, the reconstructed shower core position is required to be inside the array. The later results demonstrates the ability to reach an effective area of  $\sim 1000 \text{ m}^2$  for showers with an energy of 100 GeV.

### 5.2. Shower core position reconstruction

The shower core position is obtained by using the signal recorded by the WCD stations applying a strategy similar to the one described in [32]. The shower core is obtained by fitting a 2 dimensional lateral density distribution (LDF) to the WCD data. The fitting function parameters were derived using the average gamma 2D-LDF measured at ground by the WCDs. It was found a rather universal behaviour with the shower energy and so the parameters were fixed at all energies. The initial guess to the 2D-fit, which has as free parameters the position  $(x_c, y_c)$  and a normalisation, is provided by the calculation of the signal barycentre. The procedure described above allows to obtain a good reconstruction of the core which, as expected, improves as the shower energy increases (see figure 6). At 200 GeV the core resolution is about 20 m, while at 1 TeV the shower core can be reconstructed with an accuracy better than 3 m.

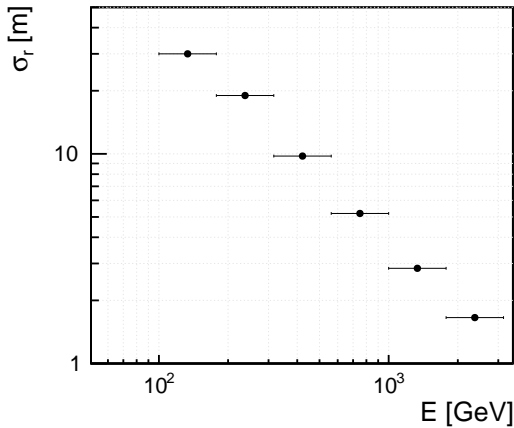


Figure 6: Shower core position reconstruction resolution for gamma-ray primaries as a function of the reconstructed energy.

### 5.3. Shower geometric reconstruction

The arrival direction of the primary particle can be achieved by exploring the arrival time of the shower secondary particles to the ground. For this reason, for the shower geometry reconstruction, the RPCs pad position and hit time will be used. A time resolution of  $\sigma_t = 1$  ns was considered, which can be achieved by present RPCs with standard electronics. The shower arrival direction is reconstructed assuming a shower front conic model as described in [33]. This model has a parameter for the shower curvature which was extracted from gamma shower simulations. Again, no significant evolution with energy was observed and the used parameter is the same for all energies. An iterative fitting process is done until the variation in the reconstructed direction in consecutive iterations is smaller than 0.1 degree. As first estimate for the fit, the direction obtained by assuming a shower front plane model was used.

In order to improve the angular reconstruction it is required that the event has at least 10 active RPC pads. The pad is only accepted for the reconstruction if it belongs to a triggered WCD station. This cut also reduces the contamination due to low multiplicity accidentals.

Moreover, late arrival hits were removed through the application of a shower front plane model. Hits with a delay bigger than 5 ns with respect to the reconstructed shower front are discarded.

We compare the reconstructed angle with the simulated angle, and we calculate the 68% containment angle,  $\alpha_{68}$ . The results as a function of the reconstructed energy are shown in Fig. 7. As expected,  $\alpha_{68}$  decreases with the increase of the reconstructed energy reaching a value of 0.3 degrees at  $E_{rec} = 1$  TeV. A reasonable resolution, better than  $1.5^\circ$ , can be achieved at energies around 100 GeV.

### 5.4. Energy estimate

The shower energy is reconstructed from the total signal, defined as the sum of the number of photoelectrons in all triggered

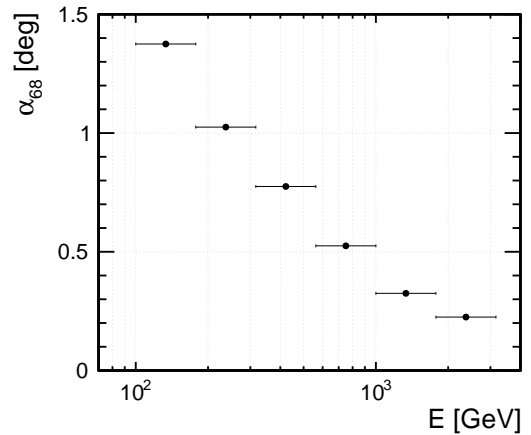


Figure 7: Angular resolution for gamma-ray primaries with zenith angle  $\theta = 10^\circ$ , as a function of the reconstructed energy.

WCD stations. The event is accepted only if the reconstructed core is inside the array. A calibration curve is obtained using the photon simulation with the Crab spectrum, by plotting the median of the generated photon energies in each bin of measured signal, as a function of the median of the measured signal (see Fig. 8, top). From this figure it can be seen that a good linearity between simulated energy and total signal can be reached even to energies below 100 GeV.

The reconstructed energy follows quite well a log-normal distribution as a function of the generated energy. The energy resolution was thus calculated by fitting the distribution of  $\ln(E/E_0)$  with a Gaussian function; the relative resolution is shown in Fig. 8, bottom. The resolution on the reconstructed photon energy depends both on the detector resolution and on the fluctuations in the shower development.

### 5.5. Hadron background suppression

The hybrid configuration of the detector units allows to combine the background rejection techniques developed by ARGO and HAWC [15, 13]. ARGO gamma/hadron (g/h) discriminators rely on the analysis of patterns at ground. These analyses rely on the use of sophisticated tools such as artificial neural networks, which is currently out of the scope of this work. However, such analysis could be imported to this detector concept, even if the RPC pads are bigger than the ARGO one's.

Hence, we wish to demonstrate that a good g/h discrimination can be achieved using solely the small water-Cherenkov detector. Among many observables tested two showed a high potential to distinguish between gamma and hadron showers, which we called:  $S_{40}^{high}/S_{40}$  and *compactness*.

The first observable is related to the presence of muons or energetic sub-showers far away from the shower core (above 40 m) in hadronic induced showers, but hardly noticeable in gamma showers. To get a grip on this quantity, we compute the total signal recorded by all WCD stations more than 40 m far from the shower core above a given signal threshold,  $S_{40}^{high}$ . This quantity, computed event-by-event, is then divided by the total

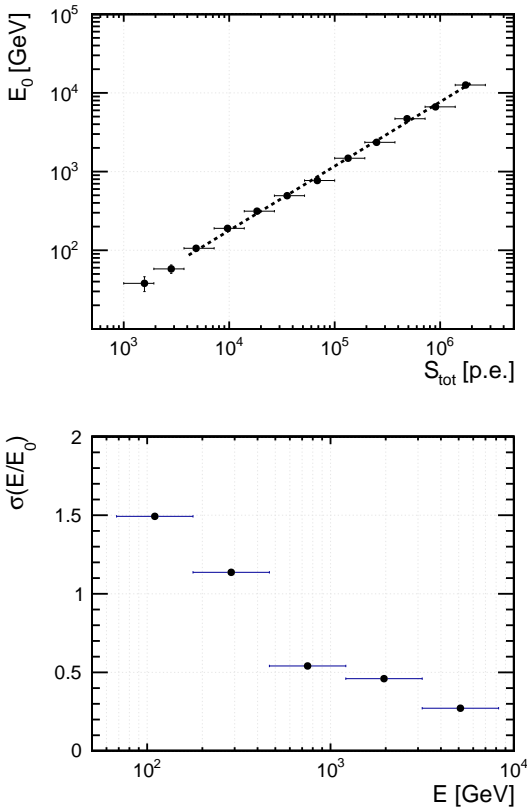


Figure 8: Top: Calibration between simulated energy and WCD signal at ground, for photons with a spectral energy distribution as for Crab Nebula. Bottom: Resolution in the reconstructed energy, for the same sample of photon-initiated showers.

signal present, in the same event, for all WCD stations more than 40 m far from the shower core,  $S_{40}$ . The signal threshold is taken as the signal that one single muon would give while crossing one WCD. Proton induced showers have in average a higher signal far away from the shower core, which means that the computed ratio ( $S_{40}^{high}/S_{40}$ ) will be greater than for gamma primaries.

The second observable is related to the shower lateral distribution function (LDF) steepness, which is higher for gamma induced showers. An average LDF for gamma showers was obtained for each reconstructed energy bin. This LDF, with no free parameters except one normalisation factor, is then fit to the event and the sum of the difference between the WCD data points and the fitted function is used as an estimator for the nature of the primary. It is worth noting that, while developed independently, similar g/h discrimination strategies were applied by the HAWC collaboration [32].

In order to maximize the discrimination factor the two discrimination variables were combined using a linear discriminant (Fisher analysis).

The results of this exercise are presented in Fig. 9. Here, it is shown the selection efficiency after applying the gamma/hadron cuts. For each energy bin, the cut value of the discriminant variable was chosen in order to maximize the ratio of the sig-

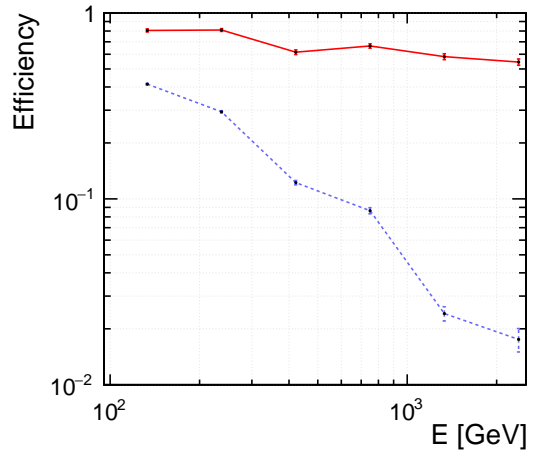


Figure 9: Gamma/proton showers selection efficiency as a function of the reconstructed energy. Gammas are shown by the red (full) line while protons appear as blue (dashed).

nal (gammas) over the square root of the background (protons). From this, it can be seen that the rejection of protons increases rapidly as the shower energy increases, while the gamma selection efficiency remains above 50%. The calculation of the sensitivity was done using a monotonous smoothed curve of figure 9 to reduce statistical fluctuations. The obtained curves for the signal and background efficiencies are within the computed statistical uncertainties.

### 5.6. Significance of the Crab signal

Gamma-initiated events have been selected within the angular window defined by the cone with half-aperture equal to the angular resolution for photons. The cosmic-ray background has been calculated for the same window, assuming an isotropic flux. Protons are reconstructed with all the analyses procedures developed for gammas. For instance, the calibration curve obtained for photons is used to derive the event energy either it is a gamma or a proton. Due to the limited simulation statistics at the highest energies the sensitivity is only computed up to 2 TeV. The event rate in each bin of reconstructed energy, before background suppression, is shown in the top plot of Fig. 10.

We then computed the number of events for one year of effective time, after applying the hadron suppression efficiency curves; the result is shown separately for signal and background events in the bottom plot of Fig. 10. One year of effective time corresponds to  $7.9 \times 10^6$  seconds, assuming a duty cycle of 25% (which corresponds to the average fraction of time at which a source culminating at zenith is seen within an angle of  $30^\circ$  from zenith).

The significance of a detection in terms of number of standard deviations  $n_\sigma$  can be calculated with a simplified formula  $n_\sigma \simeq N_{\text{excess}} / \sqrt{N_{\text{bkg}}}$ , where  $N_{\text{excess}}$  is the number of excess events, and  $N_{\text{bkg}}$  is the background estimate, whenever  $N_{\text{excess}} \ll N_{\text{bkg}}$ . For  $N_{\text{excess}} \leq N_{\text{bkg}}$  the sensitivity calculation should be done in another premisses. The significance of the

Crab signal for one year is also shown in the bottom plot of Fig. 10.

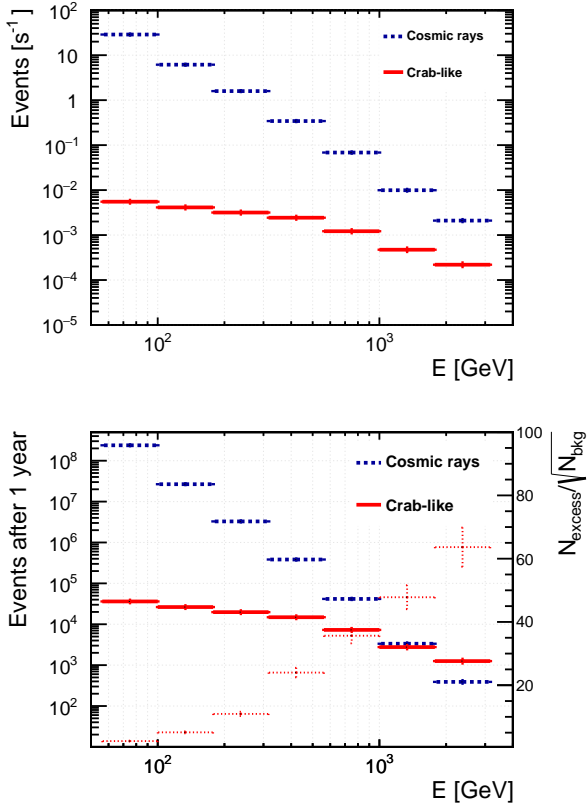


Figure 10: Top: Expected event rate in LATTES from a Crab-like source at a zenith angle of  $10^\circ$  (solid line) and the background from charged cosmic rays (dashed line) after the selection in the  $1\sigma$  angular region, before the background rejection. Bottom: Expected number of events from a Crab-like source (solid line) and background (dashed line) in one year of effective observation time after all cuts. The significance, expressed as the ratio between the signal and the square root of the background, is also shown.

### 5.7. Sensitivity for a steady source

To evaluate the performance of the detector, we compute its differential sensitivity. To accomplish this we investigate the sensitivity in narrow bins of energy (4 bins per decade). We compute the sensitivity as the flux of a source giving  $N_{\text{excess}}/\sqrt{N_{\text{bkg}}} = 5$  after 1 year of effective observation time for a source visible for 1/4 of the time (this roughly corresponds to the visibility of the Galactic Centre from the Southern tropic).

The result is shown in Fig. 11, and compared with the one-year sensitivities of *Fermi* and HAWC [32]. From this figure, it can be seen that this detector concept is in fact able to lower the energy threshold of present gamma-ray EAS experiments, with an acceptable sensitivity. It is worth noting at this point that this result comes from an end-to-end simulation.

While this result is solid, the comparison with HAWC might not be fair as a source, like the Crab Nebula, is not observed at a fixed zenith angle in the sky. In order to take this effect into account, one would need to simulate this detector concept

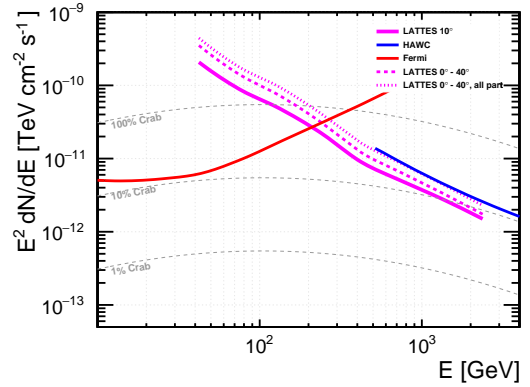


Figure 11: Differential sensitivity compared to the present sensitivity of HAWC [32] and the sensitivity of *Fermi* for observations of the galactic center [34]. The LATTES full line is the sensitivity obtained for a source at a zenith angle of  $10^\circ$ ; the dashed curve is an estimate of the LATTES performance while following the Crab Nebula transit; the thin dashed curve is an estimation of the sensitivity considering the all-particle cosmic-ray flux (see text for details). For comparison, fractions of the Crab Nebula spectrum are plotted with the thin dashed gray lines.

for other zenith angles. Such task would not only be computationally heavy but it would also require the refinement of the shower reconstruction analyses to higher zenith angles, not to bias the performance results artificially.

Hence, we decided to estimate the performance of this detector concept taking the full simulation at 10 degrees as baseline. CORSIKA photon shower simulations, equivalent to the ones generated at 10 degrees, were generated for zenith angles between 0 degrees and 40 degrees. These CORSIKA showers were then processed by a fast detector simulation, where the amount of electromagnetic energy recorded by each station was saved. Under the assumption that the reduction of the sensitivity with the zenith angle arises mainly from the decrease of the shower trigger efficiency, due to the atmospheric attenuation, a mapping between the effective area computed using the full simulation and the corresponding electromagnetic energy recorded at ground was created. With this mapping, the effective area of this array can now be estimated for other zenith angles. It should be noted that this approach was undertaken only for the photon primaries. For the background, the effective area computed from the full simulation at 10 degrees was kept. However, a reduction of the flux of cosmic rays at ground, due to the increased atmospheric attenuation, is also expected. The effective area of the background at larger zenith angles is thus overestimated and the obtained sensitivity curve is probably a conservative one. Using the effective area as a function of the zenith angle and the time a source is at a given position in the sky one can easily compute the total sensitivity of the detector accounting for the transit of the source. To ease the comparison, the Crab Nebula as seen from HAWC's latitude [35] was chosen. The obtained result can be seen in Fig. 11 as a dashed pink line. As expected the degradation in sensitivity is more important at lower energies. At the highest energies the atmospheric attenuation barely affects the trigger efficiency and the

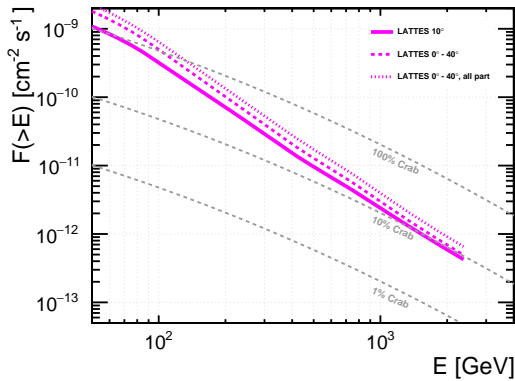


Figure 12: Integral sensitivity, defined as the flux of a source above a given energy for which  $N_{\text{excess}}/\sqrt{N_{\text{bkg}}} = 5$  after 1 year. The LATTES full line is the sensitivity obtained for a source at a zenith angle of  $10^\circ$ ; the dashed curve is an estimation of the LATTES performance while following the Crab Nebula transit; the thin dashed curve is an estimation of the sensitivity considering the all-particle cosmic-ray flux (see text for details). For comparison, fractions of the integral Crab Nebula spectrum are plotted with the thin, dashed, gray lines.

only impact on the sensitivity comes from the reduction of the array area perpendicular to the source direction.

Finally, it should be pointed that the simulated performance presented here uses for the background model the full simulation and reconstruction of the proton component. Although a full simulation of the heavier cosmic rays species was not considered here, an estimation of the expected sensitivity was also made using the all particle cosmic-ray flux from [36]. This is shown in Fig. 11 as the thin dashed curve. It should be stressed that this is a conservative estimate. In fact, the number of muons and sub-showers increases with the mass of the primary cosmic-ray, allowing for a better discrimination of the hadronic background. As such the sensitivity, computed using a full simulation and reconstruction of the remaining background components, is expected to be better than the curve shown above.

The differential sensitivity is independent of the spectral energy distribution (SED) of the emitting source. To compute the total sensitivity one must assume a SED; from this assumption, one can compute an integral sensitivity.

We compute the integral sensitivity as the flux of a source with a SED proportional to the SED of the Crab Nebula giving  $N_{\text{excess}}/\sqrt{N_{\text{bkg}}} = 5$  after 1 year, and integrating all energies above a given energy. The integral sensitivity is shown in Fig. 12.

### 5.8. Discussion on the hybrid concept

The hybrid nature of the proposed detector concept is the key ingredient for its performance, in particular at the lowest energies. It allows to decouple the calorimetric energy measurement of the shower particles at ground, using the WCD detectors, from the measurement of their time, provided by the RPCs. In fact, the detector energy threshold can be lowered by increasing the light collection efficiency, and thus the total WCD signal. This can be achieved by employing a highly reflective material to cover the inner walls of the WCDs. The main drawback is the

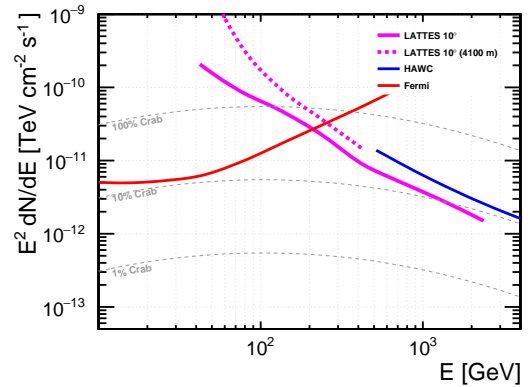


Figure 13: Same as figure 11, including the LATTES sensitivity curve computed for an altitude of 4100 m.

increase of the light collection time and the consequent degradation of the WCD time resolution. In our case, with the timing being provided by the RPCs, this is no longer an issue.

Furthermore, the trigger is based solely on the compact array of small sized WCDs. Since RPCs are sensitive to low energy charged particles, by removing the RPCs from the trigger, one avoids spurious triggers, namely due to the soil radioactivity. This allows also to reduce the energy threshold of the detector.

In order to better evaluate the impact of the present detector concept with respect to the gain expected by going to high altitudes, the differential sensitivity of the array placed at 4100 m was computed from a full simulation for low energy showers and is compared with the sensitivity at 5200 m in figure 13. Although a degradation of the performance is observed, as expected, the sensitivity is kept towards the low energies, down to about 100 GeV.

## 6. Summary

We have proposed a novel, large field-of-view, hybrid, extensive air shower detector sensitive to gamma rays of energies starting from 100 GeV (or even less for special high flux transients), based on individual units made (from top to bottom) by:

- a thin slab of lead, to allow conversion of secondary photons in showers into electron-positron pairs;
- a position-sensitive detector like a RPC;
- a water Cherenkov detector (or any other electromagnetic calorimeter with some muon identification capabilities).

We have shown that such a detector, if deployed on a surface of some 20 000 m<sup>2</sup>, can reach a sensitivity that can provide the missing link between *Fermi* and HAWC, between 100 and 350 GeV. Such detector would be able to detect in one year with a  $5\sigma$  significance a source as faint as the Crab Nebula at 100 GeV. Above 1 TeV it could reach sensitivities better than 10% of the Crab Nebula flux.

The instrument is able to survey half of the sky, with enhanced ability to detect transient phenomena making it a very powerful tool to trigger observations of variable sources, in particular flares by active galactic nuclei, and to detect transients coupled to gravitational waves and gamma-ray bursts.

An external sparse array of units could be easily achieved, due to the modular nature of the detector. This would not only allow to extend the energy range but also would further improve the sensitivity of the core array at lower energies.

The presented hybrid detector concept is currently the baseline design of the core array of the LATTES project, foreseen as a new EAS gamma-ray detector in the Southern hemisphere, complementary to the planned Cherenkov Telescope Array.

## Acknowledgements

The authors thank B. De Lotto for her comments on the manuscript.

R. Conceição acknowledges the financial support given by Fundação para a Ciência e Tecnologia, Portugal. U. Barres de Almeida is funded by a CNPq Produtividade em Pesquisa 2 Grant Nr. 309306/2013-6 from Brazil. His work on this project is partially funded by a FAPERJ Thematic Grant Nrs. 210.951/2015 and 110.148/2013 from the State of Rio de Janeiro.

## References

- [1] A. De Angelis, M. Pimenta, *Introduction to particle and astroparticle physics* (Springer, 2015)
- [2] B. Degrangé, G. Fontaine, *Comptes Rendus Physique* **16**, 587 (2015)
- [3] S. Funk, *Ann. Rev. Nucl. Part. Sci.* **65**, 245 (2015), 1508.05190
- [4] A.M. Hillas, *Astropart. Phys.* **43**, 19 (2013)
- [5] F. Acero et al. (Fermi-LAT), *Astrophys. J. Suppl.* **218**, 23 (2015), 1501.02003
- [6] M. Ackermann, et al. (Fermi-LAT), *Astrophys. J.* **222**, 5 (2016)
- [7] A.U. Abeysekara, et al. (HAWC), *Astrophys. J.* **817**, 3 (2016)
- [8] L. Fuhrmann, et al., *MNRAS* **441**, 1899 (2014)
- [9] F. Aharonian, et al. (HESS), *Nature* **531**, 476 (2016)
- [10] A. Loeb, *Astrophys. J.* **819**, L21 (2016), 1602.04735
- [11] W.B. Atwood, et al., *Astrophys. J.* **697**, 1071 (2009)
- [12] M. Amenomori, et al. (Tibet-AS $\gamma$ ), *Adv. Space Res.* **47**, 629 (2011)
- [13] B. Bartoli et al. (ARGO-YBJ), *Astrophys. J.* **779**, 27 (2013)
- [14] J. Pretz, (for HAWC), in *Proceedings, 34th International Cosmic Ray Conference* (2015)
- [15] A.U. Abeysekara, (for HAWC), in *Proceedings, 34th International Cosmic Ray Conference* (2015)
- [16] G. Di Sciascio, (for LHAASO), in *Cosmic Ray International Seminar: The status and the future of the UHE Cosmic Ray Physics in the post LHC era (CRIS 2015)* (2016)
- [17] N. Budnev et al., *JINST* **12**, C08018 (2017)
- [18] A.M. Hillas, in *19th ICRC (La Jolla), Vol 3, 445* (1985)
- [19] G. Dubus et al., *Astropart. Phys.* **43**, 317 (2013), 1208.5686
- [20] P. Abreu, (for AUGER), in *Proceedings, 34th International Cosmic Ray Conference* (2015)
- [21] D. Heck et al., *FZKA-6019* (1998)
- [22] A. Ferrari et al., CERN-2005-010, SLAC-R-773, INFN-TC-05-11 (2005)
- [23] T. Böhlen et al., *Nuclear Data Sheets* **120**, 211 (2014)
- [24] S. Ostapchenko, *Phys. Rev.* **D83**, 014018 (2011)
- [25] S. Agostinelli et al., *Nucl. Instrum. Meth.* **A506**, 250 (2003)
- [26] J. Allison, et al., *IEEE Trans.Nucl.Sci.* **53**, 270 (2006)
- [27] T.C. Weekes et al., *Astrophys. J.* **342**, 379 (1989)
- [28] A.A. Abdo et al., *Science* **331**, 739 (2011)
- [29] M. Tavani et al., *Science* **331**, 736 (2011)
- [30] J. Aleksić et al. (MAGIC), *JHEAp* **5-6**, 30 (2014)
- [31] C. Patrignani et al. (Particle Data Group), *Chin. Phys.* **C40**, 100001 (2016)
- [32] A.U. Abeysekara et al., *Astrophys. J.* **843**, 39 (2017), 1701.01778
- [33] A.K. Calabrese Melcarne, G. Marsella, D. Martello, L. Perrone, S. Sbano (ARGO-YBJ), *Temporal and spatial structure of the extensive air shower front with the ARGO-YBJ experiment*, in *Proceedings, 32nd International Cosmic Ray Conference (ICRC 2011): Beijing, China, August 11-18, 2011* (2011), Vol. 1, pp. 66–69
- [34] W. Atwood et al. (Fermi-LAT), *Pass 8: Toward the Full Realization of the Fermi-LAT Scientific Potential* (2013), 1303.3514, <http://inspirehep.net/record/1223837/files/arXiv:1303.3514.pdf>
- [35] Astropy Collaboration, T.P. Robitaille, E.J. Tollerud, P. Greenfield, M. Droettboom, E. Bray, T. Aldcroft, M. Davis, A. Ginsburg, A.M. Price-Whelan et al., *A&A* **558**, A33 (2013)
- [36] H.P. Dembinski, R. Engel, A. Fedynitch, T. Gaisser, F. Riehn, T. Stanev, *PoS ICRC2017*, 533 (2017), 1711.11432